



HAL
open science

Charged particle signatures of the diamagnetic cavity of comet 67P/Churyumov–Gerasimenko

Zoltan Nemeth, J. Burch, C. Goetz, R. Goldstein, Pierre Henri, C. Koenders, H. Madanian, K. Mandt, P. Mokashi, I. Richter, et al.

► **To cite this version:**

Zoltan Nemeth, J. Burch, C. Goetz, R. Goldstein, Pierre Henri, et al.. Charged particle signatures of the diamagnetic cavity of comet 67P/Churyumov–Gerasimenko. *Monthly Notices of the Royal Astronomical Society*, 2016, 462 (Suppl 1), pp.S415-S421. 10.1093/mnras/stw3028 . insu-01404126

HAL Id: insu-01404126

<https://insu.hal.science/insu-01404126>

Submitted on 17 Mar 2017

HAL is a multi-disciplinary open access archive for the deposit and dissemination of scientific research documents, whether they are published or not. The documents may come from teaching and research institutions in France or abroad, or from public or private research centers.

L'archive ouverte pluridisciplinaire **HAL**, est destinée au dépôt et à la diffusion de documents scientifiques de niveau recherche, publiés ou non, émanant des établissements d'enseignement et de recherche français ou étrangers, des laboratoires publics ou privés.

Charged particle signatures of the diamagnetic cavity of comet 67P/Churyumov–Gerasimenko

Zoltan Nemeth,^{1★} J. Burch,² C. Goetz,³ R. Goldstein,² P. Henri,⁴ C. Koenders,³ H. Madanian,⁵ K. Mandt,² P. Mokashi,² I. Richter,³ A. Timar¹ and K. Szego¹

¹Wigner Research Centre for Physics, Konkoly-Thege M. Road 29-33, 1121 Budapest, Hungary

²Division of Space Science and Engineering, Southwest Research Institute, 6220 Culebra Road San Antonio, TX 78238, USA

³Institut für Geophysik und extraterrestrische Physik, TU Braunschweig, Mendelssohnstraße 3, D-38106 Braunschweig, Germany

⁴Centre National de la Recherche Scientifique (CNRS), Laboratoire de Physique et Chimie de l'Environnement et de l'Espace, Orléans, France

⁵Department of Physics and Astronomy, University of Kansas, 1450 Jayhawk Blvd. Lawrence, KS 66045, USA

Accepted 2016 November 21. Received 2016 November 18; in original form 2016 June 30

ABSTRACT

One of the scientific objectives of the *Rosetta* mission is to investigate the diamagnetic cavity of comet 67P/Churyumov–Gerasimenko. We employed combined data of several instruments of the Rosetta Plasma Consortium to identify and study diamagnetic cavity crossing events. Using electron data from the Ion Electron Sensor to complement the Magnetometer data enabled us to work out a search criterion for the cavity crossing events based on a unique signature we identified in the electron spectrum. Although this search criterion is insufficient to find all the cavity events, we were able to find an abundance of more than one hundred cavity crossings in the data obtained in the summer of 2015. This unexpectedly high number of events allowed us to study their common features, as well as the shape and extent of the diamagnetic cavity in the terminator plane. The results suggest that in the summer of 2015 there was a cavity around comet 67P, which had a highly variable outer boundary. We present the effects of the diamagnetic cavity on the thermal and suprathermal electron and suprathermal ion content of the plasma, and also the probable mechanisms responsible for these charged particle signatures.

Key words: magnetic fields – plasmas – methods: data analysis – comets: individual: 67P/Chuyumov–Gerasimenko.

1 INTRODUCTION

Cometary magnetospheres show strong resemblance to the magnetospheres of non-magnetic Solar system bodies, with notable differences due to the gas outflow from the nucleus and its subsequent ionization, and the significant changes in their distance from the Sun (Russell et al. 1982). The upstream region is also strongly influenced by the ionization of neutrals. Depending on the size of the comet magnetosphere, this does or does not affect the magnetosphere proper. For a comparison of strong, intermediate and weak comets, see section 4 of Szegő et al. (2000), where the authors used the opportunity provided by the encounters with 1P/Halley, 21P/Giacobini–Zinner and 26P/Grigg–Skjellerup to compare the magnetospheres of these three very different comets.

The interaction of cometary material with the solar wind leads to the formation of several interesting structures (Szegő et al. 2000; Mandt et al. 2016), some of which have equivalents near other

nonmagnetic bodies as well, while some are unique to comets. The formation of a bow shock is characteristic; however, comets sometimes lack this feature. Although a strong interaction between the solar wind and comet Giacobini–Zinner was observed on 1985 September 11 during the flyby, no evidence for a conventional bow shock was found as ICE entered and exited the regions of strongest interaction of the solar wind with the cometary environment (Bame et al. 1986). In the magnetohydrodynamic model described in Galeev, Cravens & Gombosi (1985), the condition of shock formation is that the loaded solar wind decelerated to Mach number $M = 2$. If this number is higher, a bow wave is formed.

Behind the bow-shock/bow-wave at all comets very complex regions can be found. Deep inside the cometary magnetosphere there is a region called the diamagnetic cavity, from which outflowing plasma expels the magnetic field (Cravens 1987; Ip & Axford 1987). At Halley, a narrow (50 km) transition layer exists at the cavity boundary at which the plasma density was observed by the *Giotto* IMS to be enhanced by a factor of about 3 (Goldstein et al. 1989), as shown in their fig. 6. The existence of this enhancement was

* E-mail: nemeth.zoltan@wigner.mta.hu

predicted by Cravens (1989) and was explained as being due to the pile-up of cometary ions that flow outwards from the cavity and collide with the magnetic barrier. The electron temperature profiles also show sharp temperature increases in the inner coma, albeit at $r \approx 15\,000$ km rather than at $r = 10\,000$ km. The temperature rise is associated with the thermal collisional decoupling of the electron and ion gases from the neutral flow (Körösmezey et al. 1987).

The electrons and ions are strongly coupled to the neutral gas in the inner coma where the neutral density is high and where the electron–neutral and ion–neutral energy exchange rates are large. All the temperatures are about the same inside the cavity: $T_e \approx T_i \approx T_n$. The electron and ion temperatures become significantly higher than the neutral temperature only at larger values of r . The neutral temperature initially decreases due to adiabatic cooling as the gas expands outwards from the nucleus, but further out T_n increases due to photochemical heating. At Comet Halley, the electron temperature is equal to T_n for r less than about 2000 km but then increases rapidly for two reasons: (1) reduced electron–neutral cooling at large distances and, (2) heating from Coulomb collisions of the thermal electrons with the suprathermal (energies $E \approx 10$ eV) photoelectrons (Cravens 1987; Körösmezey et al. 1987). Heat conduction significantly reduces the electron temperature by transporting heat away from larger cometocentric distances down to the collision-dominated inner coma where the electrons are more efficiently cooled. The ion and electron structures at the boundary will be discussed in the next section.

Before the *Rosetta* mission (Glassmeier et al. 2007b) only the magnetosphere of Halley was explored more than once by three probes registering different structures due to the variable SW conditions and emission rate (due to rotation). The three flyby orbits were similar; they inclined about 107° to the Sun–nucleus line, but the closest approach distances were different, 8000 km in the case of the two VEGAs, and 500 km for *Giotto*, hence only *Giotto* could enter into the magnetic cavity (Neubauer et al. 1986). The distance from the nucleus was 4470 km upon entering and 4155 km upon exiting the cavity; the distance spent inside the cavity along the orbit was 8513 ± 7 km. The measured cavity boundaries were sharp. Inside the cavity the density of the dominant cometary ion component fall as $1/r$. Outside the cavity it returned to $1/r^2$.

On 1992 July 10, exploring comet Grigg–Skjellerup, *Giotto* crossed the bow shock of the comet and entered the dust coma about 17 000 km from the nucleus (Neubauer et al. 1993). Closest approach occurred at a distance of 330 km (Richter et al. 2011), the spacecraft passed by the nucleus on the night side. It was the closest ever cometary flyby before *Rosetta*. An abrupt shock wave was detected on *Giotto*’s outbound leg, but was not clearly identified on the inward journey (Neubauer et al. 1993). Magnetic field strength was slightly higher there than at Halley, but no diamagnetic cavity was detected around the much smaller nucleus.

At 67P/Churyumov–Gerasimenko (67P), we have not yet detected the bow shock or any indication of it. The solar wind was deflected by cometary ions, but no significant deceleration was observed (Behar et al. 2016). In the magnetosphere, low-energy cometary ions were continuously seen flowing out from the nucleus, and a medium energy cometary ion component arriving from roughly the solar direction was also detected (Nilsson et al. 2015a,b). The cavity was first detected on 2015 July 26 (Goetz et al. 2016b); the distance of the cavity boundary was much larger than that predicted by recent models (Gombosi 2015; Koenders et al. 2015; Rubin et al. 2015; Huang et al. 2016). As the cavity diameter is still much smaller than at Halley, not only the gradient

of the magnetic pressure, but also the field curvature participate in the pressure balance between the magnetic field and the ion–neutral drag, which makes this result even more puzzling.

Here, we report the finding of more than a hundred cavity crossing events, by using a method, which combines the data of several particle detectors and the magnetometer of the Rosetta Plasma Consortium (RPC). Based on this event-set, we investigated the properties of the vicinity of the cavity boundary, and also the possible shape and extent of the diamagnetic cavity in the terminator plane.

We note that this intermittent set of short crossing events is very different from the classical cavity observation near 1P/Halley, where *Giotto* remained for a long time continuously inside the cavity. The cause of the difference is not clear yet. *Giotto* crossed the magnetosphere of Halley at high speed, and thus may have missed the dynamics of the cavity boundary. Perhaps the cavity boundary of comet 67P is more dynamic. It is even possible that these short cavity-like events are not connected to a global diamagnetic cavity, but are due to some local effects, which cause similar magnetic and plasma signatures. It may be more appropriate to call them magnetic dropout events, but (as we will show) their particle signatures are also very ‘cavity like’, thus we will refer to these events as ‘cavity crossings’, with the caveat that these may not be detection of a classical global Halley-type cavity, but possibly that of local events. The decision about whether we see the dynamic boundary region of a global cavity or local cavities is beyond the scope of this paper and needs further research.

2 OBSERVATIONS AND METHODS

After the first detection of 67P’s diamagnetic cavity (Goetz et al. 2016b) by the RPC Magnetometer (MAG) (Glassmeier et al. 2007a), we investigated the plasma properties around and inside the cavity using the data of several RPC instruments. RPC features a complete set of plasma instruments (Carr et al. 2007) and is able to measure a wide range of plasma properties.

The chief instrument of cavity detection is naturally the magnetometer, but as *Rosetta* is a ‘magnetically dirty’ spacecraft, large and varying magnetic disturbances on board the spacecraft make the magnetometer calibration very difficult. Thus some uncompensated residual field of the spacecraft may remain after precalibration, and the obvious criterion for cavity detection (namely the very small field amplitude) may not work well for cavity crossings occurring when the s/c residual field was comparable to the measured field values. As the field is expelled from the cavity that region should be magnetically quiet, which means that the field fluctuations dominating the measurements outside the cavity should also be lacking inside. Thus, finding extended time intervals featuring an approximately constant magnetic field is also an indication of cavity events (Goetz et al. 2016b) but the search may be complicated by relatively large uncompensated residual fields.

We investigated whether other sensors of RPC can aid the search for cavity events, specifically the data of the Ion Electron Sensor (IES) electrostatic analyser (Burch et al. 2007) and the Mutual Impedance Probe (MIP; Trotignon et al. 2007). We found a very distinct cavity signature in the IES electron dynamic spectrum (see the second panel of Fig. 1). There is a well-defined component of the electron energy spectrum around 150–200 eV, which drops abruptly when the spacecraft enters the cavity. These electron signatures can be easily identified in the dynamic spectrum, which makes them an ideal tool for cavity search. These drop-outs are usually accompanied by an attenuation of the 100 eV electron component, which is also a common feature of the electron spectrum near the

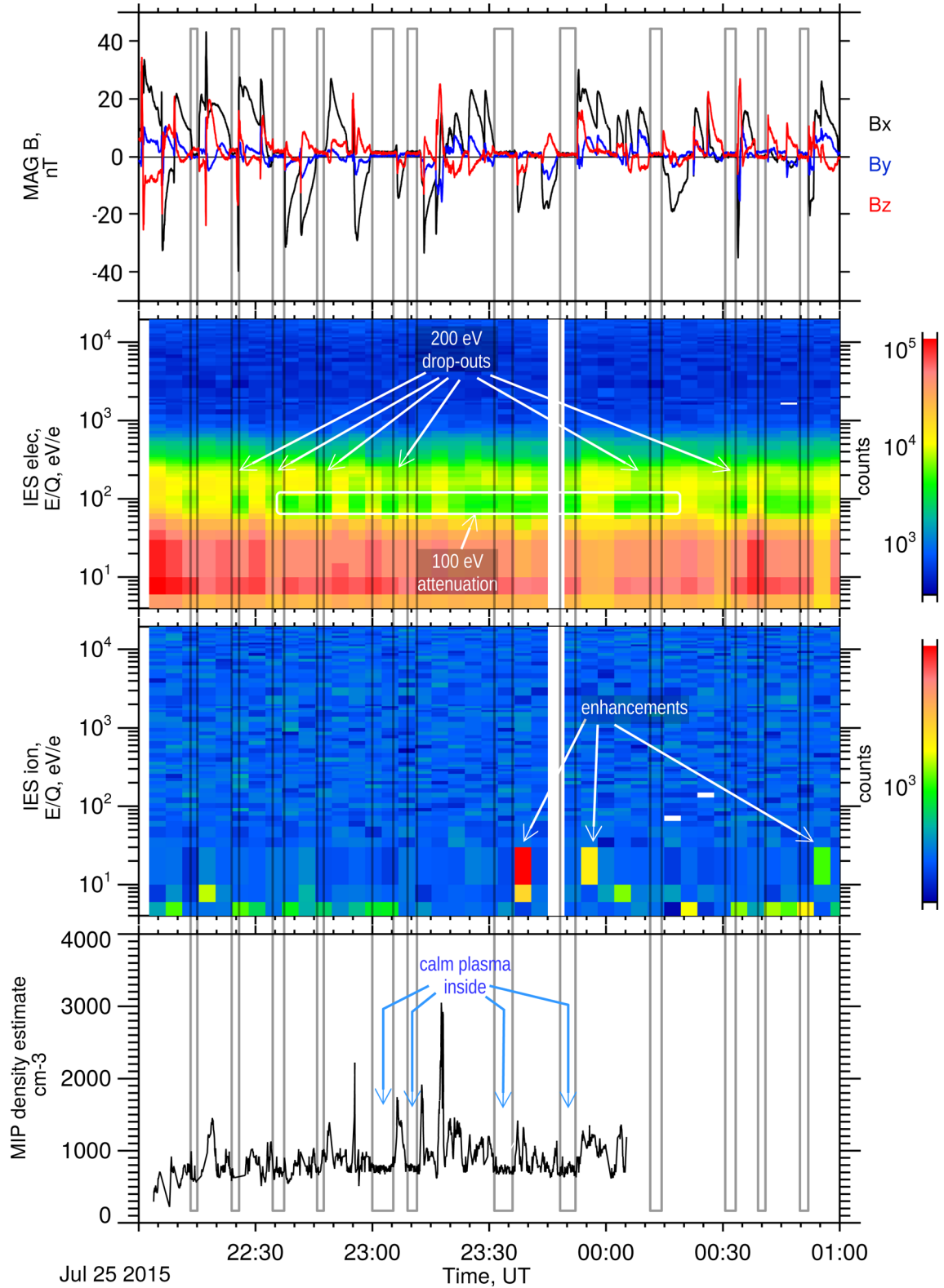


Figure 1. Magnetic field, IES electron, IES ion spectra and MIP density estimate from July 25 22:00 to July 26 01:00. The x , y and z components of the magnetic field are shown as black, blue and red lines in the upper panel. Calibrated field values are shown with residual fields removed. Grey rectangles mark the positions of some of the cavity crossings. Two distinct features of the electron spectrum accompany cavity crossings. Long attenuation periods of the energetic component around 100 eV (showing as a green ‘stripe’ from e.g. 22:30 to 00:15) are common in the vicinity of the cavity. Short periods, where the 150–200 eV component drops by about a factor of 2 (greenish rectangles in a yellow stripe, some marked by white arrows) coincide with the magnetic signatures of the cavity. The ion spectrum features enhancements in the cavity boundary in the 10–40 eV energy range. The thermal electron density as measured by the Mutual Impedance Probe (MIP) shows calm unperturbed plasma inside the cavity, and strong density increases in the cavity boundary.

cavity. These attenuation events however usually last much longer than the actual cavity crossings. They indicate that we are close to the cavity, but not necessarily inside it. A sharp drop-out in the 150–200 eV component inside a longer 100 eV attenuation interval is a very good indication of cavity crossing.

We searched the IES electron data of 2015 June, July and August for cavity signatures. Where we found the characteristic 200 eV drop-outs, we checked the level of magnetic field fluctuations. If all three field components were approximately constant (although not necessarily zero) during the drop-out, we considered the event as a cavity candidate. If there were several cavity candidates close to each other, and all of them had the same field values, we deduced that we observe cavity encounters there, but with a significant uncompensated residual field vector (sometimes as large as 30 nT), which is constant throughout several cavity crossings. In these months, these electron signatures always indicated cavity crossings (magnetic dropout signatures) as well, although earlier during the mission we can see somewhat similar electron behaviour without magnetic signatures.

In summary, our search criteria were: 1) short drop-outs in the 150–200 eV component of the electron spectrum usually during longer 100 eV attenuation events; 2) accompanied by ‘cavity-like’ magnetic signatures: no or very small fluctuations around a constant value for all three magnetic field components simultaneously; 3) verified by other similar events, which have the same residual field values. We shall return to the theoretical justification of these conditions later.

Using this method, we identified more than a hundred (127) cavity crossings. This search criterion is not sufficient to find all the cavity events; it favours longer multiple events featuring relatively stable residual magnetic fields. Our method can only identify cavity crossing events longer than 1 min. Nevertheless, we can build an event data set, which can serve as a basis for better calibration of the magnetic field data, which in turn opens up the possibility to detect shorter cavity crossings as well using a more traditional field amplitude criterion. Goetz et al. (2016a) performed an analysis of recalibrated high-resolution magnetic field data. For the time period, we studied (2015 June, July and August) the two methods give very similar event sets, which suggests that in the time period we studied, the particle signatures are concomitant with the magnetic dropout events.

Fig. 1 shows a typical example: 12 cavity crossing events within 3 h. Recalibrated field data (Goetz et al. 2016b) are shown in the first panel, which feature very small (less than 3 nT) residual field values inside the cavity. The residual field values in this period were -7 , -11 and 6 nT for the x , y and z components, respectively, in the time of our original cavity search. The 150–200 eV drop-outs can be readily observed in the electron spectrum of the second panel. The figure also shows a longer attenuation in the 100 eV electron energy range. These longer attenuation events often accompany (surround) the cavity events; they seem to be a characteristic feature of the plasma near cavity encounters, probably associated with higher neutral densities. It is difficult to identify the ion signatures, although the measured count rate and the energy of the thermal ion component inside the cavity is somewhat lower – this may be associated with changes in spacecraft potential (Odelstad et al. 2015). The ion count rate sometimes shows strong enhancements in the boundary layer of the cavity, elsewhere the limited field of view of the sensor may prevent the detection of the ion enhancements in the cavity boundary. The time resolution of the particle sensors is not high enough to resolve the thickness and detailed structure of the boundary layer of the cavity. The last panel shows the MIP

density, which estimates the plasma density from the plasma frequency identified in the active complex (both amplitude and phase) mutual impedance spectra of the MIP experiment, here operated in the so-called SDL mode. In this time period, the density is around 800 cm^{-3} inside the cavity and features very little fluctuations there, but it shows strong enhancements in the cavity boundary, where the density is two to four times higher. Some examples of these charged particle signatures are indicated by arrows in the figure.

3 COMMON FEATURES OF CAVITY CROSSING EVENTS

The first striking result we can deduce from our event set is that there are a lot of cavity crossings this far from the comet. It rules out the possibility that the detection of the cavity by the *Rosetta* spacecraft was a result of a singular low-probability event such as a huge outburst of the comet. *Rosetta* encounters the cavity quite regularly, while flying 150–300 km away from the nucleus. Transient effects may still play a role in these cavity crossings, but we need to refine the theoretical and numerical models alike to be able to explain these frequent crossings.

Analysing the distribution of these events we can observe that short few minutes long (in–out) crossings are most common, but we can find longer encounters as well, in which the spacecraft stays inside the cavity for several minutes, including 3, which are longer than 15 min, 8 in the 10–15 min range and 25 in the 5–10 min range. The events are often grouped together, see Fig. 1 for an example, where 12 cavity events occurred within 3 h around midnight July 25–26.

The magnetic field close to the cavity crossing events is dominated by a strong x component in the comet centred solar equatorial (CSEQ) coordinate system. (The origin of this frame is the comet’s centre of mass; the $+X$ -axis is the position of the Sun relative to the body, the vector points from the body to the Sun; the $+Z$ -axis is the component of the Sun’s north pole of date orthogonal to the $+X$ -axis; the $+Y$ -axis completes the right-handed reference frame.) This means that in the vicinity of the cavity the field drapes around the obstacle as expected. The peak-to-peak amplitude of B_x is roughly 40–80 nT. About one third of the events coincide with abrupt changes of the magnetic field direction. As close to the cavity the field features frequent and strong directional variation without cavity crossings as well, the variation in and out of the presence of the cavity may have a common origin. (Variations of the interplanetary magnetic field piled-up in front of the nucleus or instabilities of the contact surface disturbing the magnetic field close to the cavity for example.) Comparing the field immediately before entering the cavity (B_{in}) and after exiting the cavity (B_{out}) reveals strong scatter, but as a rule B_{in} shows the same tendency as B_{out} , meaning that entering and leaving the cavity in general happen in similar magnetic environments. For a more detailed analysis of the magnetic environment of the vicinity of the cavity, see Goetz et al. (2016a). We found that the residual field is changing slowly along the path of *Rosetta*; but there are also sharp changes accompanying the attitude variations of the spacecraft. The x component of the residual field is usually small (a few nanotesla), the y and z components can be as large as 20–25 nT.

The thermal electron density as measured by the MIP shows very calm unperturbed plasma inside the cavity, and strong (two- to three-fold) density increases in the cavity boundary, see the bottom panel of Fig. 1 for a few examples of this behaviour. The density inside the cavity changes smoothly during this month from 500 cm^{-3} in the beginning of the month up to 1000 cm^{-3} at the end of July, where

it starts decreasing again. The in situ large-scale density variation over July is most likely driven by the changing activity of the comet peaking a few weeks after perihelion, although possibly it is also modulated by the spacecraft trajectory around the comet. The average ratio of the densities inside the cavity and in the cavity boundary is 0.5, but the peaks are sometimes very high, the maximum in this time interval was about 6000 cm^{-3} . The peaks detected entering and leaving the cavity are usually of similar size (the average of the ratio of the in and out peaks is 1) but they show strong variation.

The energetic electron count rates in the 150–200 eV energy range (which serve as the basis of our search criterion) are two to three times lower inside the cavity than immediately outside. The counts of the electrons around 100 eV drop somewhat more strongly, but this drop is also present where the spacecraft is outside the cavity but close to its boundary. Thus, the features in the 100 eV component can be used to find those time periods, when the spacecraft was in the vicinity of the cavity, while the signature in the 150–200 eV component indicates the cavity itself. For a detailed study of the full electron spectrum, see Madanian et al. (2016a).

The IES ion spectrum does not feature such distinct cavity signatures as the electron spectrum, but the low-energy ion component shows a decrease in energy and also in count rate inside the cavity. We can also often observe ion enhancements inside the cavity boundary in the 10–40 eV energy range, some of these are pointed out in the third panel of Fig 1. Similar variations of the ion spectrum were observed earlier accompanying changes in the spacecraft potential (Edberg et al. 2015; Odelstad et al. 2015), which suggests the possibility that the features in the ion spectrum may be the result of the variation of the spacecraft potential, and thus indirectly the result of the change in the electron distribution.

4 SPATIAL DISTRIBUTION OF THE EVENTS – THE EXTENT OF THE CAVITY

The intermittent nature of the cavity observations together with the unexpectedly high distance from the nucleus, at which these observations were performed, raise the question whether there is a global cavity of several hundred km radius around the nucleus or local enhancements of the density and velocity of the neutral atmosphere and/or the dust cloud (e.g. jets) cause small localized cavities. Either global or local, it is a primary goal of the *Rosetta* mission to determine the extent and shape of the diamagnetic cavity. The multitude of cavity encounters in the summer of 2015 allows us to study and at least partially answer these questions.

The coloured line in the top panel of Fig. 2 shows the orbit of *Rosetta* in the terminator plane (the y - z plane of the CSEQ coordinate system) in this time period. The spacecraft flew near the terminator plane along a path consisting of long ballistic (almost straight) segments connected by short direction changing manoeuvres. The bottom panel shows the distance from the comet. We marked the location of cavity encounters by black + signs on both panels. The first conclusion to draw from the figure is that cavity crossings are rather common at this distance from comet 67P and in this time period. There is no single specific direction favoured by the events, they are not the results of uncommonly large outbursts or jets, there are lots of them along this part of the spacecraft trajectory. All the crossing events are short (point-like on this time-scale), in sharp contrast with the continuous cavity observation at Comet Halley.

As we mentioned earlier the observed distance of the cavity boundary from the nucleus was much larger than that predicted by recent models. The cavity crossings were detected in the

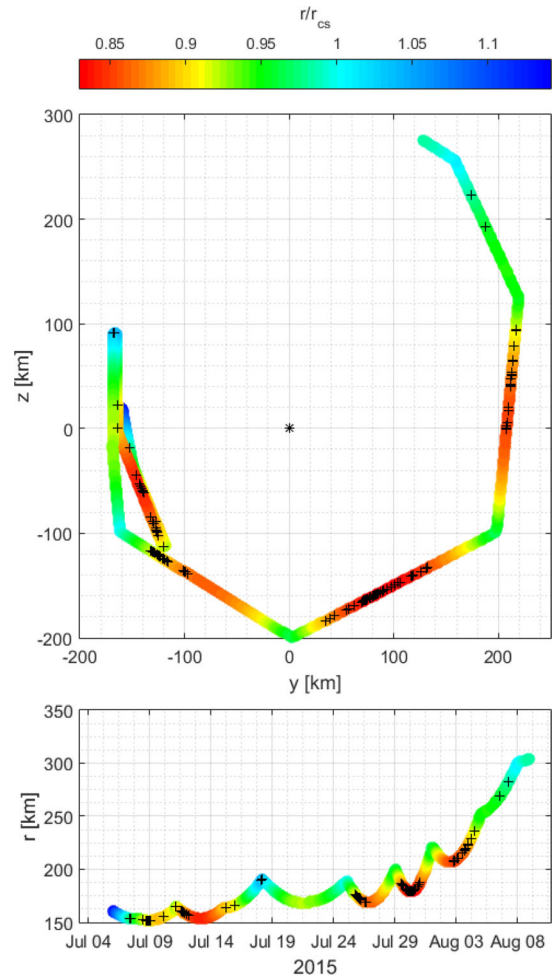


Figure 2. Top panel: the orbit of *Rosetta* (coloured line) in the y - z plane of the CSEQ coordinate system; bottom panel: the distance between *Rosetta* and the nucleus. Black + signs mark the sites where *Rosetta* encountered the cavity; the colour of the lines represent the distance from the nucleus in r_{cs} units, where r_{cs} is the time dependent theoretical boundary distance (see the text).

150–300 km range. It is worth noting however that the original simple neutral drag model of Cravens (1986) provides results in very good agreement with the observations. According to this model, the cavity stand-off distance scales as $r_{cs} \sim Q^{3/4}/B$, where Q is the gas production and B is the characteristic magnetic field amplitude in the cavity boundary. If we take the same gas production rate as used in Koenders et al. (2015) and Rubin et al. (2015) $Q = 5 \times 10^{27} \text{ s}^{-1}$ and scale the stand-off distance of the cavity of Comet Halley ($r_{cs} = 4400 \text{ km}$ at $Q = 6.9 \times 10^{29} \text{ s}^{-1}$ and $B = 50 \text{ nT}$) by this value, we get $r_{cs} = 110 \text{ km}$. Higher production rates, e.g. $Q = 8 \times 10^{27} \text{ s}^{-1}$ as used in Huang et al. (2016) can reproduce higher distances. Fig. 2 shows observations for more than a month, during which time the comet approached its perihelion. During this period, the cometary activity increased significantly (Jäckel et al. 2015), which could cause higher densities, which in turn would lead to an extension of the cavity due to an increased neutral drag term in the model of Cravens (1986, 1989). A factor of 3 increase in gas production would be enough to push the cavity boundary outwards by about a factor of 2. We used a production rate estimate function $Q(t)$ based on comet rotation averaged ROSINA water production rates detrended for spacecraft location (Hansen et al. 2016) to compute

the theoretical boundary distance (r_{cs}) by scaling the (Cravens 1986) result with $Q(t)^{3/4}$. We coloured the spacecraft trajectory on Fig. 2 by r/r_{cs} . Thus, the line colour indicates the distance from the nucleus in r_{cs} units, where r_{cs} is the time-dependent theoretical boundary distance. We did not scale with B here, which means that we did not take into account the effects of magnetic field variations in the draping region. These variations (induced by variations of the solar wind dynamic pressure) also play an important role in determining the stand-off distance (Madanian et al. 2016a).

Closer examination of the data reveals a structure in the spatial distribution of cavity crossing events. We can see that they are grouped together on those parts of each ballistic segment, which are closer to the comet (see the lower panel of Fig. 2). Parts of the segments further away from the comet are free from the events, *Rosetta* did not encounter the cavity there. More specifically, the red and yellow parts of the trajectory (where the spacecraft is closer to the comet than 0.9 times the boundary distance predicted by this simple theoretical model) are most likely to harbour cavity crossing events. Thus, the Cravens (1986) model describes the extent of the cavity quite well, but instead of finding a continuous cavity inwards the position of the theoretical boundary we find intermittent event trains there. Also, there are some red parts of the trajectory lacking crossing events and a few events can be found further away as well. The model in its simplest form cannot account for these findings.

The intermittent in–out nature of the cavity encounters can be caused by either a breathing motion of the cavity boundary or ripples on it; a combination of the two is also possible. In extreme cases, instead of ripples an instability of the contact surface can even manifest itself in ‘magnetic rain’: drops of magnetized plasma detached from the outer region and moving inside the cavity. Such magnetic rain was observed at Venus (Brace et al. 1983) earlier. To decide between these possibilities an analysis of the high-resolution magnetic field and plasma data is required.

5 ORIGIN OF THE PARTICLE SIGNATURES

We observed an energetic electron population, which drops sharply when the spacecraft enters the cavity. The drop is quite significant, and the count rates decrease at least by a factor of 2 on the boundary. This suggests an electron population bound to the field lines, which is not inherent to the cavity region but reaches the vicinity of the cavity together with the field lines. As the field lines are expelled from the cavity, so is this field line bound electron population.

On the origin of this field line bound population we can only speculate. The energy region is appropriate for strahl electrons, but the count rates are much higher than that of the electron strahl in the solar wind. Their abundance suggests that this is a population accelerated in the vicinity of the comet from a lower energy abundant seed population, such as the electrons born in the ionization processes of the coma, and picked up by the solar wind there. Due to the huge size of the cometary atmosphere, the field lines entering the dense inner regions are already significantly loaded by matter of cometary origin. This plasma comprises photoelectrons generated further away from the comet. Those electrons are formed at around 10–15 eV, so a 10- to 15-fold acceleration can produce the observed 150–200 eV population. These electrons probably undergo a ‘betatron-like’ acceleration mechanism due to the compression of the magnetic field as the flow enters the draping region. This follows from the conservation of the first adiabatic invariant: if B increases, the perpendicular energy of the electrons must increase as well to maintain the invariance of the magnetic moment. As the interplanetary magnetic field reaches the pile-up region it is compressed,

and so the electrons picked up in the tenuous outer atmosphere of the comet are accelerated, their energy multiplied by the magnetic compression factor. This is consistent with the observations as the magnetic field compression ratio and the electron energy gain factor with respect to photoelectrons are roughly the same. If the electrons really were accelerated by this betatron-like mechanism, then their energy should correlate with the magnitude of the magnetic field. Such correlation was discovered by Broiles et al. (2016), who performed a statistical analysis of the suprathermal electron populations around comet 67P. Their result strongly supports our hypothesis, although other acceleration mechanisms may also be responsible for (or play a role in) the formation of this field line bound electron population.

In the observations of the MIP experiment, we witness density enhancements in the thermal electron plasma of cometary origin as the flow penetrates the magnetic field. Due to the small gyroradius of these low-energy electrons, the magnetic field traps them at the very edge of the cavity boundary. The electron density builds up in this region, from which the electrons can only exit by slow processes. These thermal peaks might also be related to the thermalization of and/or ionization by suprathermal electrons (Madanian et al. 2016b). The plasma density inside the cavity is free of significant fluctuations, which means that the interaction with the neutral flow smooths out the plasma, and/or that there are no such processes inside the cavity, which perturb the plasma and generate plasma inhomogeneities. The density inside slowly changes with time together with the neutral density in accordance with expectations, as the source of this plasma is the ionization of the neutral gas. Supposing for example photochemical equilibrium and roughly constant ionization rates, the electron density is predicted to be proportional to the square root of the neutral density (Cravens 1987).

An enhancement of the ion density is to be expected in quasi-neutral plasma to compensate the electric charge resulting from the electron density increase. This rule is also applicable here, although in absence of electric fields the ions would decouple from the electrons when the plasma enters the magnetized region, because due to their much larger gyroradius the ions do not ‘feel’ the magnetic field until they penetrate the boundary by tens of kilometres. However, quasi-neutrality is restored by an electric field on scales larger than the Debye length (which is only about 10 cm here), because a relatively small charge imbalance can self-consistently build up a polarization (ambipolar) electric field, which entraps the ions in the vicinity of the cavity boundary. Thus, the thermal ion density cannot deviate far from the electron density. Although IES only detects ions with energies higher than 4 eV, this effect should lead to lower ion counts inside the cavity and enhancements in the cavity boundary in accordance with the observations.

It is more difficult to determine the origin of the ion energy signatures. As the energy enhancement is very localized, most of the acceleration processes can be ruled out. Even strong fields and localized acceleration would result in such a suprathermal population, which would inevitably leak out of the acceleration region and enter either the cavity or the outer parts of the cavity boundary. To explain the observations, this population should be present only at the edge of the cavity boundary, and should travel together with this edge. Currently, we consider it more probable that these ion events reflect the changes in the spacecraft potential when entering the narrow region of high electron density described in the previous paragraph. A high enough negative spacecraft potential can accelerate the ions from the vicinity of *Rosetta* into the detectors with the observed energies. The spacecraft potential is determined by a current balance: the current resulting from impacting electrons is an important factor

of this balance and high electron densities can generate strong negative potentials (Odelstad et al. 2015). Similar ion enhancements were found earlier by Goldstein et al. (2015), who pointed out that these ions must be newly produced near the s/c and attracted by its negative potential. They are often well correlated with the local neutral density and electron flux. When the potential is not negative enough these ions are not seen. The spacecraft potential can also play a role in the variation of the ion count rates because IES only sees ions with energies above a threshold (≈ 4 eV), and a stronger potential can accelerate more cold ions into the measurement range of the instrument. This mechanism is localized to regions of high electron current (such as the edge of the cavity) and also to the spacecraft – and thus can explain the lack of these ions elsewhere.

6 CONCLUSIONS

In this paper, we have shown that particle signatures of the diamagnetic cavity can provide an important aid for finding cavity crossing events. We constructed a search criterion based on the cavity signatures discovered in the IES electron spectrum, which can be used to find these events even in the presence of changing magnetic field residual fields resulting from stray fields of the spacecraft. We used this criterion to find 127 cavity crossing events in the data measured in the summer of 2015.

In this time period, the spacecraft never entered the cavity for more than half an hour, but there were lots of shorter crossings. Our method can only identify cavity crossing events longer than 1 min. Most of the 127 events were short few minutes long crossings, 25 of them were 5–10 min long, 8 were in the 10–15 min range and there were 3 longer than 15 min. The events are often grouped together along the spacecraft trajectory, while other parts of the orbit are free of cavity events. The recurrent crossings may be the result of either a breathing motion or ripples on the cavity boundary. The distance from the comet at which the cavity is detected is larger than that predicted by recent models (Gombosi 2015; Koenders et al. 2015; Rubin et al. 2015; Huang et al. 2016), but it is in good agreement with the simple theoretical model of Cravens (1986, 1989).

We identified distinct cavity signatures in both the thermal and suprathermal electron populations as well as in the ion spectrum. The drop-outs in the suprathermal electron population is interpreted as the result of this population being bound to the field lines. These electrons are accelerated in the magnetic pile-up region, most likely by a betatron-like mechanism, gyrate along the field lines, and thus are expelled from the cavity together with the field lines. The thermal plasma density peaks at the edge of the cavity because as the plasma flowing from the direction of the nucleus enters the magnetized region the field immediately traps its electron component. These density peaks probably lead to enhancements of the electron current charging the spacecraft, and the resulting strongly negative spacecraft potential can accelerate ions into the detector, which is the most probable cause of the detection of 20–40 eV ion bursts near the edge of the cavity.

ACKNOWLEDGEMENTS

Rosetta is an ESA mission with contributions from its member states and NASA. We thank the Rosetta Mission Team, SGS and RMOC for their outstanding efforts in making this mission possible. The work on IES was supported, in part, by the U.S. National Aeronautics and Space Administration through contract 1345493 with the Jet Propulsion Laboratory, California Institute of Technology. Work at LPC2E/CNRS was supported by CNES and by ANR under the financial agreement ANR-15-CE31-0009-01. The work of

ZN was supported by the János Bolyai Research Scholarship of the Hungarian Academy of Sciences. The work on RPCMAG was financially supported by the German Ministerium für Wirtschaft und Energie and the Deutsches Zentrum für Luft- und Raumfahrt under contract 50QP 1401. Data analysis was partially performed with the AMDA science analysis system provided by the Centre de Données de la Physique des Plasmas (CDPP) supported by CNRS, CNES, Observatoire de Paris and Université Paul Sabatier, Toulouse.

REFERENCES

- Bame S. et al., 1986, *Science*, 232, 356
 Behar E., Nilsson H., Wieser G. S., Nemeth Z., Broiles T. W., Richter I., 2016, *Geophys. Res. Lett.*, 43, 1411
 Brace L. H., Taylor H. A., Jr, Gombosi T. I., Kliore A. J., Knudsen W. C., Nagy A. F., 1983, in Hunten D. M., Colin L., Donahue T. M., Moroz V. I., eds, *Venus. Space Science Series*. Univ. Arizona Press, Tucson, AZ, p. 779
 Broiles T. W. et al., 2016, *MNRAS*, 462, S312
 Burch J. L., Goldstein R., Cravens T. E., Gibson W. C., Lundin R. N., Pollock C. J., Winningham J. D., Young D. T., 2007, *Space Sci. Rev.*, 128, 697
 Carr C. et al., 2007, *Space Sci. Rev.*, 128, 629
 Cravens T. E., 1986, in Battrick B., Rolfe E. J., Reinhard R., eds, *ESA SP-250: ESLAB Symposium on the Exploration of Halley's Comet*. European Space Agency (ESA), Paris, p. 241
 Cravens T. E., 1987, *Adv. Space Res.*, 7, 147
 Cravens T. E., 1989, *J. Geophys. Res.*, 94, 15025
 Edberg N. J. et al., 2015, *Geophys. Res. Lett.*, 42, 4263
 Galeev A. A., Cravens T. E., Gombosi T. I., 1985, *ApJ*, 289, 807
 Glassmeier K.-H. et al., 2007a, *Space Sci. Rev.*, 128, 649
 Glassmeier K.-H., Boehnhardt H., Koschny D., Kürt E., Richter I., 2007b, *Space Sci. Rev.*, 128, 1
 Goetz C. et al., 2016a, *MNRAS*, 000, 000
 Goetz C. et al., 2016b, *A&A*, 588, A24
 Goldstein B. E., Altwegg K., Balsiger H., Fuselier S. A., Ip W.-H., 1989, *J. Geophys. Res.*, 94, 17251
 Goldstein R. et al., 2015, *Geophys. Res. Lett.*, 42, 3093
 Gombosi T. I., 2015, *Physics of Cometary Magnetospheres*. Wiley, Hoboken, NJ, p. 169
 Hansen K. C. et al., 2016, *MNRAS*, 000, 000
 Huang Z. et al., 2016, *J. Geophys. Res. (Space Phys.)*, 121, 4247
 Ip W.-H., Axford W., 1987, *Nature*, 325, 418
 Jäckel A. et al., 2015, *Proc. Eur. Planet. Sci. Congress*, Nantes, France, 2015 September 27 to October 2. Available at: <http://meetingorganizer.copernicus.org/EPSC2015/EPSC2015-545.pdf>
 Koenders C., Glassmeier K.-H., Richter I., Ranocha H., Motschmann U., 2015, *Planet. Space Sci.*, 105, 101
 Körösmezey A. et al., 1987, *J. Geophys. Res.*, 92, 7331
 Madanian H. et al., 2016a, *AJ*, in press
 Madanian H. et al., 2016b, *J. Geophys. Res. (Space Phys.)*, 121, 5815
 Mandt K. E. et al., 2016, *MNRAS*, 462, S9
 Neubauer F. M. et al., 1986, *Nature*, 321, 352
 Neubauer F. M. et al., 1993, *A&A*, 268, L5
 Nilsson H. et al., 2015a, *Science*, 347, aaa0571
 Nilsson H. et al., 2015b, *A&A*, 583, A20
 Odelstad E. et al., 2015, *Geophys. Res. Lett.*, 42, 10
 Richter I., Koenders C., Glassmeier K. H., Tsurutani B. T., Goldstein R., 2011, *Planet. Space Sci.*, 59, 691
 Rubin M., Gombosi T. I., Hansen K. C., Ip W.-H., Kartalev M. D., Koenders C., Tóth G., 2015, *Earth Moon Planets*, 116, 141
 Russell C. T., Luhmann J. G., Elphic R. C., Neugebauer M., 1982, in Wilkening L. L., ed., *IAU Colloq. 61: Comet Discoveries, Statistics, and Observational Selection*. Univ. Arizona Press, Tucson, AS, p. 561
 Szegő K. et al., 2000, *Space Sci. Rev.*, 94, 429
 Trotignon J. G. et al., 2007, *Space Sci. Rev.*, 128, 713

This paper has been typeset from a \LaTeX file prepared by the author.